Yan *et al. Energy Mater.* **2025**, *5*, 500087
DOI: 10.20517/energymater.2024.271

Energy Materials

Article

Open Access

Check for updates

Unveiling the pattern and progression of reaction extent heterogeneity inside graphite electrodes through real-time monitoring of current density

Ziwen Yan, Li Wang*, Xiangming He*

Institute of Nuclear & New Energy Technology, Tsinghua University, Beijing 100084, China.

Correspondence to: Prof. Li Wang and Prof. Xiangming He, Institute of Nuclear & New Energy Technology, Tsinghua University, A317 Nengkelou, Qinghuayuan, Haidian District, Beijing 100084, China, E-mail: wang-l@tsinghua.edu.cn; hexm@tsinghua.edu.cn

How to cite this article: Yan, Z.; Wang, L.; He, X. Unveiling the pattern and progression of reaction extent heterogeneity inside graphite electrodes through real-time monitoring of current density. *Energy Mater.* **2025**, *5*, 500087. https://dx.doi.org/10.20517/energymater.2024.271

Received: 30 Nov 2024 **First Decision:** 5 Feb 2025 **Revised:** 12 Feb 2025 **Accepted:** 18 Feb 2025 **Published:** 22 Apr 2025

Academic Editor: Jiazhao Wang **Copy Editor:** Ping Zhang **Production Editor:** Ping Zhang

Abstract

To improve electrode performance, understanding the complex changes within electrodes when working is vital. The lithiation process in graphite electrodes involves the influx of Li ions from the separator and electrons from the current collector, coupled with materials' hindrance for charged particle movement, leading to reaction extent heterogeneity. Since capacity is the cumulative effect of current density, real-time monitoring of current density to investigate reaction pathways in different sections of the electrode can enhance our knowledge of the pattern of heterogeneity as the rate increases and progression of reaction extent heterogeneity, aiding in developing mitigation strategies. This study used a pouch cell with a multilayer graphite electrode to monitor current density in real time, revealing patterns associated with increasing rates and the progression of reaction extent heterogeneity inside graphite. The results show that with rate increasing, the current density inside graphite becomes more heterogeneous, leading to more severe reaction extent heterogeneity. Besides, it is shown that heterogeneous current density leads to lithiation of top part in graphite. The resulting additional capacity released from lithium deposition will compensate for the unused capacity of the remaining layers. Consequently, for the graphite, safety has been weakened and lithium inventory has decreased while total capacity remains almost unaffected during the first lithiation.

Keywords: Reaction extent heterogeneity, graphite, real-time monitoring, state of charge heterogeneity

INTRODUCTION

The widespread application of lithium (Li)-ion batteries in increasingly complex and advanced fields has necessitated the development of batteries with superior comprehensive performance. As the primary energy-providing component in Li-ion batteries, electrodes are at the forefront of efforts to achieve longer lifespan, higher safety, and improved rate capabilities. Beyond enhancing material properties, it is crucial to address heterogeneous issues within electrodes, particularly reaction extent heterogeneity.

The academic community has gained a clear understanding of the origins of reaction extent heterogeneity[1]. During the lithiation of electrodes, ions enter from the separator side while electrons are supplied by the current collector. However, ions move within the electrode significantly slower than in the pure electrolyte due to the hindrance posed by particles, binders, and conductive additives[2]. Moreover, the electronic conductivity of the electrode is compromised by the imperfect contact between particles and conductive additives[3]. These factors contribute to heterogeneous concentration distributions of charged species throughout the electrode, leading to varying reaction rates at different locations and, consequently, reaction extent heterogeneity.

The heterogeneous reaction extent at the electrode scale can precipitate deleterious outcomes due to localized overreaction. Consider the scenario where an electrode is intended to be at 50% state of charge (SOC). Certain areas may be overcharged, while others may remain undercharged. Initially, cathode particles, such as layered materials including $Li_xNi_yMn_zCo_{(1-y-z)}O_2$ (NMC) and lithium cobalt oxide (LCO), and olivine materials such as lithium iron phosphate (LFP), may undergo structural alterations when subjected to overcharging conditions[4]. Similarly, overcharging in graphite electrodes markedly elevates the risk of lithium plating[5]. Although the fragmentation of certain particles may not immediately impair performance, continuous cycling leads to the exposure of new surfaces from fragmentation and differentiation, which can react with the electrolyte. This reaction triggers the formation of an additional solid electrolyte interphase (SEI)[6], occupying pore space, diminishing capacity, and impeding ion transport[7]. Additionally, lithium-plated graphite will inevitably interact with the electrolyte[8], exert pressure on the separator and raise safety issues[9]. The electrolyte may also react with these defect sites, potentially leading to by-product interactions[10]. Ultimately, these secondary reactions can spiral out of control, causing a rapid buildup of gases and heat, resulting in battery swelling and increasing the risk of thermal runaway[11].

As researchers delve deeper into the complexities of battery technology, they confront the multifaceted issue of reaction extent heterogeneity within electrodes. Perpendicular to the current flow direction, the distribution of this heterogeneity is often irregular, as highlighted in a recent paper[12]. This irregularity is attributed to the heterogeneous blending of electrode materials. In contrast, along the current flow direction, three distinct patterns of heterogeneity typically emerge, believed to arise from the imbalance of ions and electrons originating from opposite ends of the electrode. The diverse manifestations of heterogeneous reaction extent are closely tied to the varying structures and compositions of electrodes.

Currently, a range of techniques is employed to characterize reaction extent heterogeneity within battery electrodes. The three most prevalent methods are X-ray diffraction (XRD), X-ray absorption, and Raman spectroscopy. Since electrode materials are crystalline and exhibit distinctive infrared diffraction peaks, these techniques, when combined with experimental designs that offer spatial resolution, can translate variations in diffraction signals into spatial distribution maps of reaction extent at specific instances and track its evolution over time. To date, materials such as LFP[13,14], $LiMn_2O_4$ (LMO)[15,16], NMC[17-19], LCO[20], $LiNi_{0.80}Co_{0.15}Al_{0.05}O_2$ (NCA)[15], and graphite[21] have been investigated for their reaction extent heterogeneity

using XRD. Metallic elements such as Fe, Co, Ni, and Mn have characteristic absorption spectra in hard X-rays, which alter with changes in valence state, a feature leveraged to study reaction heterogeneity in electrodes containing these elements[22-25]. Despite the limited penetration of soft X-rays, they are promising for probing surface chemical heterogeneity[26] and, when combined with transmission X-ray microscopy, can offer detailed insights into particle reaction heterogeneity[27-29]. Raman spectroscopy is also employed for its ability to detect the unique frequencies and intensities of Raman-active bands from $Li_xNi_{1-y-z}Co_yMn_zO_2$ (NCM) lattices, making it a common choice for studying the heterogeneous SOC of NMC electrodes[7,30-32]. However, Raman spectroscopy has limitations, particularly its requirement for scanning the longitudinal profile, which hampers in-situ analysis on the electrode plane. Additional methods, such as scanning electron microscopy (SEM)[33], Kelvin probe force microscopy (KPFM)[34,35], and X-ray tomography[36], are also emerging as valuable tools for electrode heterogeneity.

Nevertheless, these tests merely reveal how the reaction extent, SOC, or capacity fluctuates over time. Delving into the deeper, underlying patterns is essential for a more comprehensive understanding, akin to uncovering a function and then exploring its derivative for a profound insight. In the context of particles, Bazant conducted a thorough analysis of scanning transmission electron microscopy (STEM) data, correlating pixel-level changes to expose the heterogeneity of the reaction process, thereby providing a deeper understanding of LFP particles[37]. For the battery as a whole, Wang *et al.* analyzed and integrated various thermal reactions, allowing the thermal change curve of the electrode to be explained as the superposition of fundamental reactions[38]. Both of these studies propose microscopic mechanisms to explain macroscopic phenomena. As for electrodes, according to kinetic equations, the products are the cumulative result of reaction rates over time, with the electrode's reaction rate defined by the current density. While the origin of reaction extent heterogeneity is clear, monitoring the current density across different regions of the electrode in real-time during charging and discharging can reveal patterns as rate increases and the progression of reaction extent heterogeneity, forming a comprehensive view of this problem [Figure 1].

In this study, a pouch cell was assembled incorporating a four-layer graphite anode, separated by thin separators, alongside an NMC cathode. Throughout the electrochemical process, the anode was lithiated at varying rates, with real-time monitoring and documentation of the current density across the four graphite layers. The analysis of the experimental data reveals that with the escalation of rates, the current density distribution becomes more heterogeneous. This distribution accumulates over time, contributing to more severe reaction extent heterogeneity. Furthermore, even though the reaction extent becomes increasingly heterogeneous with the increase of rates, lithium metal can deposit on top of graphite, thereby compensating for the capacity not released by the other layers.

EXPERIMENTAL

Materials

The graphite electrode with an areal capacity of 4.20 mAh/cm^2 (1.05 mAh/cm^2 per layer) was obtained from a slurry with the mass ratio of artificial graphite (Jiangxi Zhengtuo New Energy Technology Co., Ltd.): super P (SP): carboxymethyl cellulose (CMC): styrene-butadiene rubber (SBR) = 90:5:2.5:2.5 in appropriate amounts of H_2O. The well-mixed slurry was evenly coated on the copper (Cu) current collector with a thickness of 15 μm or copper mesh with a thickness of 9 μm, and dried in an air-circulating oven at 80 °C for 8 h. The final thickness of the graphite electrode is 36 μm after pressing. The NMC cathode with an areal capacity of 3.5 mAh/cm^2 was prepared via a similar slurry casting method on to aluminum foil, and the slurry used was NCM811: SP: polyvinyl pyrrolidone (PVP): carbon nanotubes (CNTs): polyvinylidene fluoride (PVDF) = 97.40:0.50:0.12:0.48:1.50 in appropriate amounts of N-methyl-2-pyrrolidone (NMP).

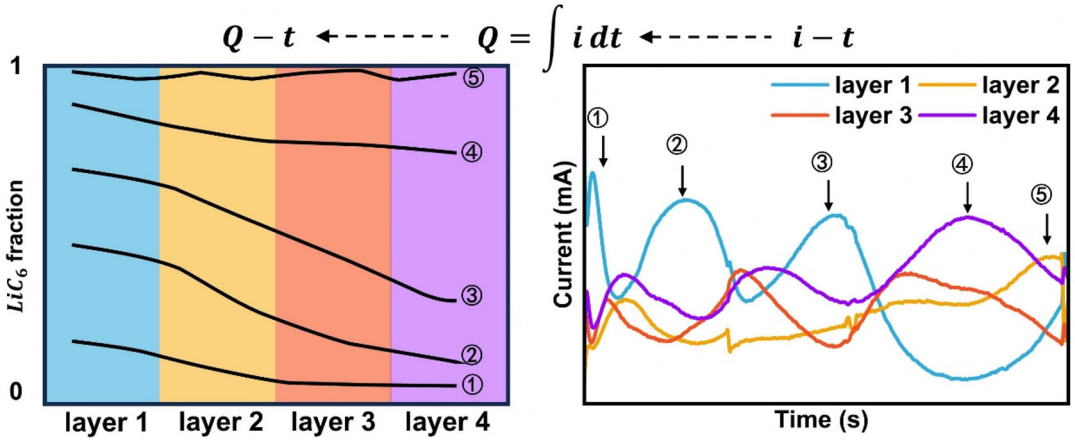

Figure 1. Because capacity is the accumulation of current over time, in order to understand the causes and development process of reaction extent heterogeneity, it is necessary to understand the current density in different parts of the electrode.

Later, the graphite electrode was cut into a square of 4 cm and the NMC electrode was cut into a square of 4.3 cm to ensure N/P plus 1 (1.04) by using a slitter and die-cutting machine. There are two types of Celgard separators here: the 24 μm one is used to isolate graphite and lithium, and the 5 μm one is used to separate graphite electrodes. The electrolyte from Beijing Institute of Chemical Reagents consists of 1 M LiPF6 in a mixture of ethylene carbonate (EC)/dimethyl carbonate (DMC)/ethyl methyl carbonate (EMC) (1:1:1, volume ratio) with 1 wt% vinylene carbonate (VC) as the additive.

Pouch cell assemblage

Pouch cells are assembled in a dry room with a dew-point temperature of less than 40 °C. The electrodes were packaged in an aluminum plastic case. The electrolyte was injected and then the cell was sealed under vacuum. After 12 h of electrolyte penetration, the batteries were charged for five hours at 0.001 A and then cycled twice at 0.025 A to form an ideal SEI. The battery cycling performance was detected by the Neware battery test system (CT-4008T-5V6A-S1, Shenzhen, China). The reference electrode for lithium plating on copper wire is arranged at the first and third layers to measure their potential in real time.

RESULTS AND DISCUSSION

The design principles of multilayer battery

The schematic diagram of the multilayer battery is shown in Figure 2 and the photo of the cell is detailed in Supplementary Figure 1. The one closest to the separator is named layer 1, downwards in order as layer 2, layer 3, and layer 4. The first three layers of graphite electrodes are placed on a copper mesh while the last layer is placed on a copper foil. Reference electrodes made by lithium-coated copper wire are placed on the first and third layers to measure the potential. Layers are separated by a 5 μm Celgard separator. The pouch cell was composed and sealed in a dry room, effectively preventing water from affecting the surface graphite and NMC[39]. The separator is meticulously positioned to maintain a distance between the copper mesh and the graphite anode surface, avoiding interaction and ensuring precise current density measurement[40].

The anode material comprises conductive graphite, enriched with a significant proportion of conductive additives (5%) and well point contact between graphite particles and SP. Each layer of graphite has a copper mesh or copper foil that provides them with electrons individually. This design principle has been experimentally proven that the electronic conductivity of this electrode is much greater than its ionic conductivity, measured by a factor of one hundred[41]. While using three separators to split thick graphite into four layers will foster electrolyte penetration, the ionic conductivity of this model electrode is still

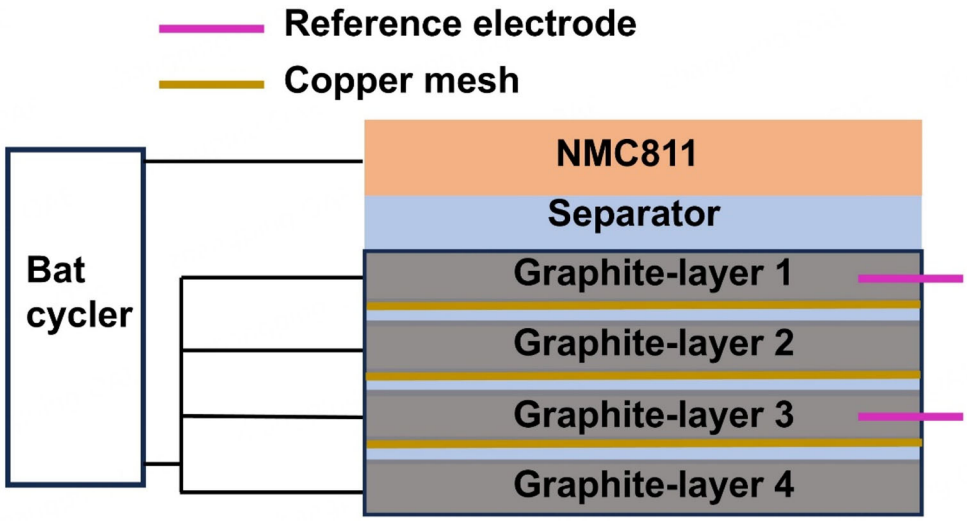

Figure 2. The schematic diagram of the multilayer battery.

reduced. The plate-like morphology of graphite particles renders them less conducive to ion conduction compared to spherical or elliptical particles, such as those found in NMC and LCO, respectively[42,43]. Moreover, the cumulative thickness of the electrode, which includes four layers of electrode material, three separator layers, and three layers of copper mesh, measures 186 μm, which is certainly disadvantageous for ion transportation[44]. Additionally, missing precise alignment of layers influences ionic conductivity, too[45]. Most importantly, ion mobility is impeded by the copper mesh. While serving as current collectors, electrons are continuously present on each layer of copper. However, in order to react with deeper graphite, ions must penetrate the copper layer through its pores even if they are repelled by electrons, which significantly slows down their movements. Taking all these factors into account, ion transport within this electrode is awesome, which justifies the slower rates adopted in this experiment, 0.05C, 0.1C, 0.2C, 0.33C and 0.5C, respectively.

In this case, compared to usual thick electrodes, this model multilayer electrode has deteriorated ionic conductivity and strengthened electronic conductivity owing to its specialized design that facilitates the measurement of current density in each layer. The concentration gradient can be intensified by increasing the operating rate or decreasing the ionic conductivity of the electrode. The ionic conductivity can be weakened by increasing thickness and decreasing porosity. Therefore, this model offers valuable insights into the principles governing ultrathick and ultradense electrodes, or electrodes operating under very high current rates.

The pattern of reaction extent heterogeneity as rate increases

Current density is inherently heterogeneous inside electrodes. During the lithiation of graphite, the reaction starts near the separator, where the reaction rate is faster[40]. As shown in Figure 3, at a rate of 0.05C, when lithiation begins, lithium ions enter the graphite electrode from the separator and diffuse into a deeper region. At this point, the ion concentration in the first layer of the electrode is higher due to materials' hindrance, resulting in a higher current density in the first layer and early completion of phase transition. The current peak profile shows that the subsequent transformations to LiC_{12} and LiC_6 follow the same order. As shown in Figure 4, analysis of the potential of the first and third layers confirms the same reaction pathway, with the first layer always reaching the phase transition potential before the third layer. The differential voltage (dQ/dV) profile in Figure 4 indicates that the reaction peaks for the first layer are higher

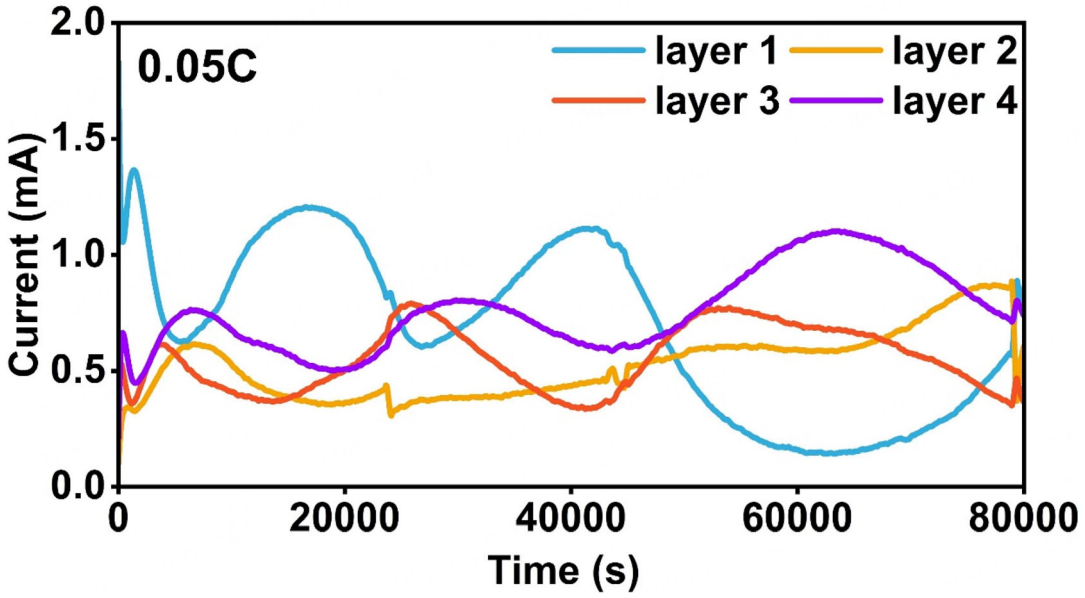

Figure 3. Current density of each layer of four-layer graphite electrode during 0.05C discharge. At relatively low cycling rates, the electrode near the separator reacts first and reacts faster due to higher ion concentration.

and narrower than those of the third layer. This is due to the hindrance of Li-ion transport by the electrode. The first layer continuously receives lithium ions from the separator end but the ions cannot quickly diffuse to the second layer and the third layer, resulting in a higher ion concentration in the first layer compared to the third layer. Therefore, the reaction rate in the first layer is higher than in the third layer when it is supposed to react. Besides, the potential plateau on the first layer is more pronounced for the same reason[40].

However, while layer 1 exhibits a clear and consistent leading transformation, the phase transition sequence in other layers appears inconsistent. The same behavior is also observed at 0.1C. The reason lies in the coexistence of heterogeneous ion concentration and potential distribution within the electrode. At relatively low rates, the ion concentration gradient is significantly less pronounced than under high-rate conditions. In this case, potential heterogeneity also plays a significant role, together with ion heterogeneity, in making the reaction path irregular.

With rate increasing, the multilayer electrode shows more pronounced ion concentration gradient and consequently current density. As illustrated in Figure 5A-E, the distribution of current density becomes increasingly more heterogeneous while overall current density increases. Because the current density is directly proportional to the ion concentration and the difference in electron concentration is very small, a more heterogeneous current density is actually due to a more heterogeneous ion distribution.

In Figure 5F, it is shown that at 0.05C, the capacity of the first and fourth layers of graphite is greater than that of the second and third layers, while at 0.2C, 0.33C, and 0.5C, the capacity decreases from layer 1 to layer 4. At 0.1C, it behaves more in a manner resembling a transition where the proportion of layer 1 increases, and the capacity of layer 4 decreases but is not less than layer 2 and layer 3. This phenomenon shares the same underlying cause as the irregular phase transition sequences observed in the other three layers excluding the first layer, under low-rate 0.05C. When rate is low, heterogeneous potential distribution also plays a significant role. However, as the rate increases, more ions rush into the graphite and ion

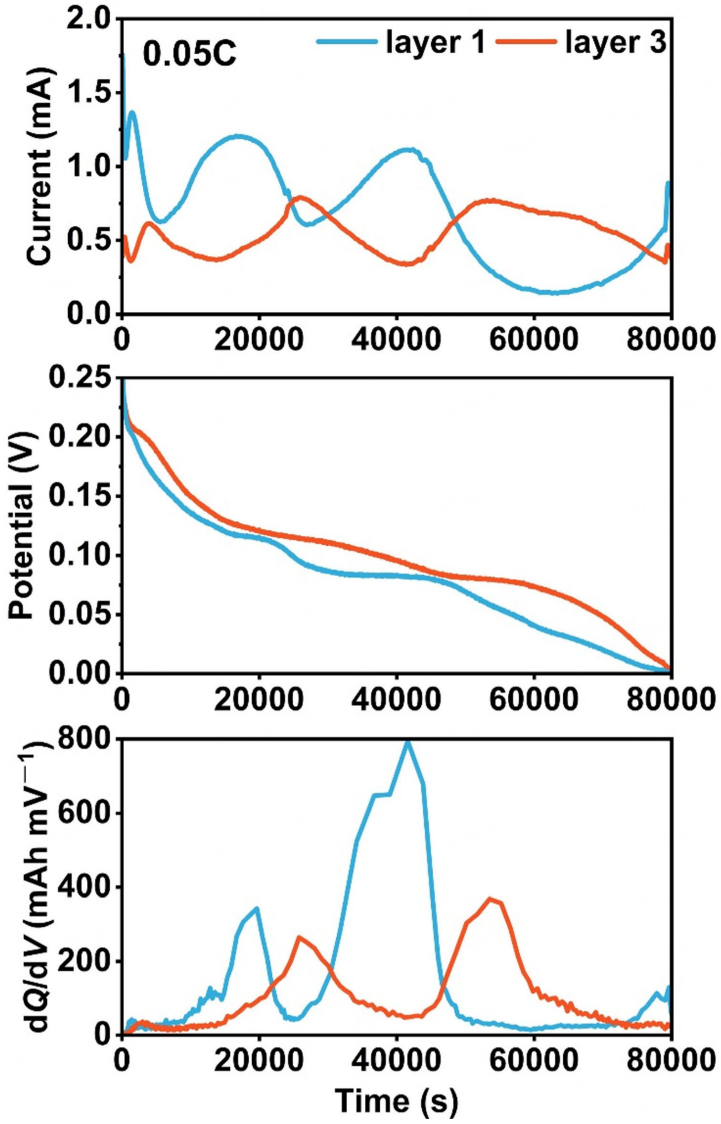

Figure 4. Comparison of current density, discharge voltage, and capacity changes between the first and third layers during 0.05C discharge.

concentration gradient becomes more pronounced, leading to the lithiation process being entirely controlled by ion diffusion.

Combining the inherently heterogeneous current density and the influences of increasing rates, the pattern of reaction extent heterogeneity is concluded. The diffusion ability of the electrode does not improve while more lithium ions enter the electrode per unit time. The consequence is that the ion concentration, which is proportional to the reaction rate, inside the electrode is more heterogeneous, leading to more heterogeneous current density distribution, accumulating to more heterogeneous reaction content.

The progression of heterogeneous reaction

There are three phenomena discovered in the lithiation process. The first phenomenon is that as rate increases, lithium deposition happens with three characteristics. First, lithium deposition only occurs in layer 1. The theoretical capacity of single-layer graphite is 16.8(±0.1) mAh. As shown in Table 1, At 0.1C,

Table 1. Capacity of each layer and total electrode capacity

	0.05C	0.1C	0.2C	0.33C	0.5C
Layer 1 (mAh)	15.147	18.349	20.714	22.965	24.370
Layer 2 (mAh)	11.651	6.290	10.143	9.108	8.867
Layer 3 (mAh)	12.257	8.393	6.034	5.033	4.523
Layer 4 (mAh)	16.909	8.387	5.772	4.224	3.656
Total (mAh)	55.964	41.419	42.663	41.330	41.420

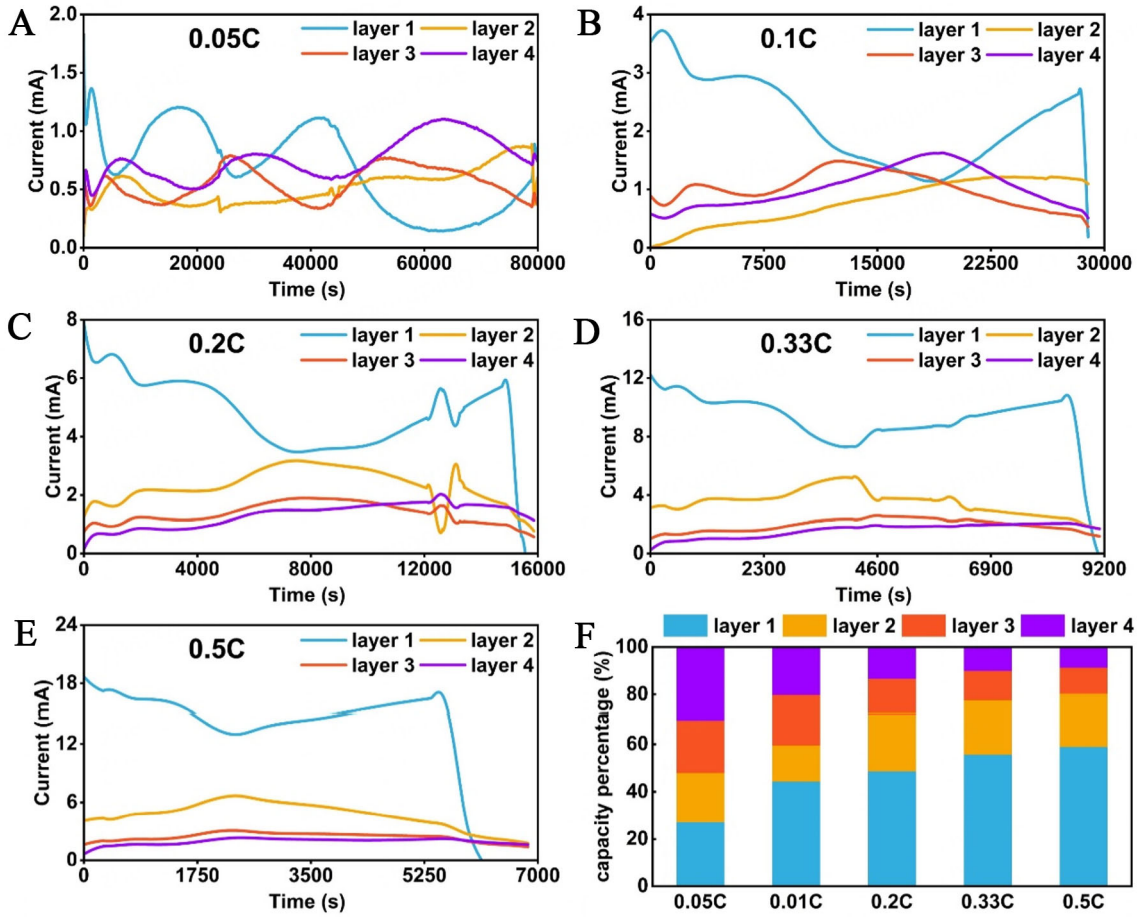

Figure 5. (A-E) The current density distribution of four layers of graphite electrodes during discharge at 0.05C, 0.1C, 0.2C, 0.33C, and 0.5C, respectively; (F) The heterogeneity of SOC during discharge of graphite electrodes increases with the increment of cycling rate. SOC: State of charge.

0.2C, 0.33C, and 0.5C, the capacity released from the first layer is greater than its theoretical capacity, while the remaining layers have not reached their theoretical capacity. However, since the potential of the second layer is not measured, whether lithium plating occurred in that layer cannot be determined. It is possible that lithium plating happens in the second layer, while the total capacity is still less than the theoretical capacity due to part of graphite has not reacted completely. The occurrence of lithium plating at relatively low rates, as previously discussed, can be attributed to the low ionic conductivity of the model electrode. Second, the amount of deposited lithium is directly proportional to the rate as the capacity of layer 1 continues to increase. Thirdly, even if lithium deposition occurs, the total SOC is still not greater than 1. The reaction lithium deposition is corroborated by in situ XRD experiments [Supplementary Figure 2].

During the resting phase after lithiation at 0.1C, 0.2C, 0.33C and 0.5C, respectively, the enhancement of the LiC_6 phase in the XRD patterns suggests that the plated metallic lithium undergoes re-intercalation over time.

The potential comparison between the first and third layers also indicates the specific occurrence of lithium deposition, as shown in Figure 6. For Layer 3, at a rate of 0.1C, it is still able to react to LiC_6, but as the cycling rate continues to increase, it can only react to LiC_{12}, indicating that a substantial portion of capacity remains unutilized. In contrast, for Layer 1, at rates of 0.1C, 0.2C, 0.33C, and 0.5C, the voltage drops significantly to 0 V, resulting in lithium deposition. It is worth noting that higher rates have more negative depositing potentials. The reason is that the ion concentration in the first layer is higher, which is consistent with the reason for the increased difference in current density mentioned above.

The second phenomenon is that, at any reaction rate except 0.05C, the current of layer 1 first decreases and then increases after a period of lithium deposition. Moreover, as the rate increases, the turning point comes faster [Figure 6]. This behavior can be attributed to several processes. First, at the beginning of lithiation, where the first layer of the electrode receives lithium ions and the second, third, and fourth layers contain no lithium ions, current density of layer 1 is maximized. Later, as Li ions diffuse into other layers, the difference of current density between layers reduces, similar to reaction pathways under 0.05C. However, the first layer of electrode continues to react at a higher rate, completing the transformation of LiC_6 first, which causes the potential of layer 1 to decrease to zero first and lithium deposition to begin. After a short period of lithium plating, metallic lithium has begun to block the pores[46,47], and the volume expansion during lithiation of graphite reduces the effective porosity, making the conduction of lithium ions more difficult[48]. This structural transformation causes relatively fewer lithium ions to diffuse into the lower layers, resulting in an increase of lithium ions in the first layer and an increase in current density owing to lithium deposition. The increasingly advanced turning point also indicates the worsening SOC heterogeneity, as the full lithiation of layer 1, along with the structural transformation, becomes faster and earlier.

The third phenomenon is that as rate increases, the capacity of whole electrodes does not significantly change. As shown in Table 1, the capacity of the first layer continues to increase, while the capacities of the second, third, and fourth layers continue to decrease, resulting in no significant change in the total capacity. For other electrode materials, the electrode will stop working in advance, resulting in a decrease in capacity, as reported in other work. Combining the worsened reaction heterogeneity with the evidence of Li deposition, the explanation of this counterintuitive phenomenon is that the first layer of graphite, which is capable of continuing reacting with Li ions to deposit metal Li on its surface after full lithiation, releases additional capacity through Li deposition to compensate unused capacity of the remaining three layers. Yet in fact, the capacity compensation caused by lithium precipitation and reaction extent heterogeneity is completely undesirable.

In this case, combining three phenomena and the inherently heterogeneous current density distribution, the progression of heterogeneous reaction extent is clear. As rate increases, the current density inside electrodes will become more heterogeneous, accumulating and resulting in more heterogeneous reaction extent. During the process, the part of electrode which is near separator will complete lithiation faster and start to deposit lithium on its surface. Coupling with structural expansion of graphite after transforming to LiC_6, ionic conductivity inside layer 1 will decrease, trapping more Li ions and promoting lithium deposition. The capacity released through lithium deposition will compensate for remaining layers that are not fully reacted. While the overall capacity does not decline, the safety[49] and lithium inventory[50] are both reduced.

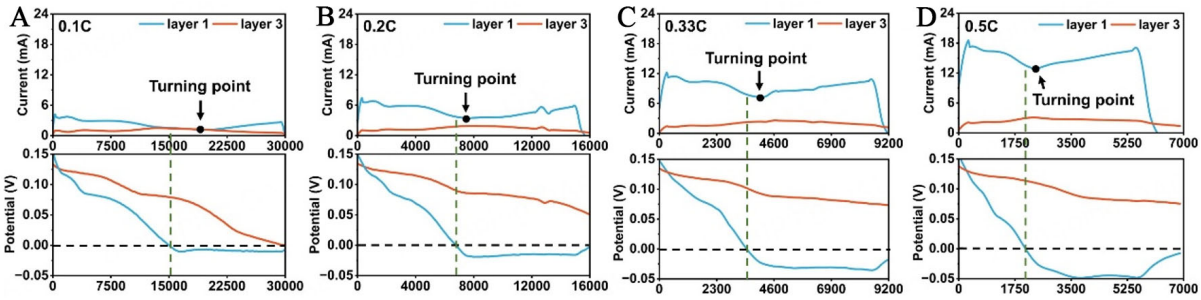

Figure 6. (A-D) The comparison of current density and potential of layer 1 and layer 3 graphite electrodes during discharge at 0.1C, 0.2C, 0.33C, and 0.5C, respectively.

Discussion and inspiration

As discussed, this study provides valuable insights for scenarios involving graphite electrodes with high tortuosity or under extremely high operating rates, where ion concentration gradients play a significant role. Without altering the material composition, increasing energy density inevitably leads to higher electrode tortuosity. Meanwhile, the ability to achieve high-rate charging and discharging offers tangible benefits for various applications, particularly in the field of electric vehicles.

Graphite particle differs from other materials such as NMC and LFP in that, even when its SOC reaches 1, it can still continue to react because lithium deposition is permissible. In this case, when studying the heterogeneous reactions in graphite electrodes, structural characterization methods such as XRD alone and description of SOC heterogeneity are insufficient[17,21], as they do not provide information on lithium deposition. Therefore, it is necessary to measure the capacity of different parts of the electrode to correctly understand the heterogeneous reaction behavior of graphite anodes.

Even if the total SOC of graphite does not reach 1, lithium deposition may still occur. As this work demonstrates, when the lower two layers of graphite have not reacted completely, the upper layers have already experienced evident lithium deposition. This finding undoubtedly provides insights for battery management, as graphite is the most commonly used commercial anode. Under fast charge and discharge conditions, more attention is required to put on the half part near the separator; more rigorous and thoughtful management protocols are required to avoid lithium deposition. Controlling solely based on capacity and cut-off voltage is insufficient, as the results show that both capacity and voltage are severely heterogeneous during the lithiation.

CONCLUSION

In summary, the pattern as rate increases and progression of reaction extent heterogeneity are investigated through real-time monitoring of current density and we have demonstrated that multilayer electrodes are powerful tools for research on reaction heterogeneity. The key findings of our research are summarized as follows.

(1) Pattern: as rate increases, ion concentration gradient becomes more significant, larger near the separator and lower near the current collector-more heterogeneous ion distribution introduces more heterogeneous current density-as time goes on, the result is more heterogeneous reaction extent.

(2) Progression: heterogeneous current density makes layer 1 complete lithiation faster and begins to deposition lithium-ion diffusion is blocked by lithium deposition and particle expansion of graphite-more

ions are trapped in layer 1, self-accelerating lithium deposition, compensating for unused capacity of remaining layers and reducing safety and lithium inventory.

DECLARATIONS

Acknowledgments

We would like to express our heartfelt gratitude to Dr. Dongsheng Ren for his guidance and contributions.

Authors' contributions

Performed methodology, investigation, experiments, data curation, and writing the original draft: Yan, Z.
Handled resources, supervision, conceptualization, and writing review and editing: Wang, L.
Contributed to conceptualization, resources, supervision, writing review and editing: He, X.
The final manuscript was reviewed by all authors and received their approval.

Availability of data and materials

The authors declare that the data supporting the findings of this study are available within the article and its Supplementary Materials files.

Financial support and sponsorship

We would like to express our gratitude to the National Natural Science Foundation of China (22279070) and the "Explorer 100" cluster system of Tsinghua National Laboratory for Information Science and Technology for their support and provision of facilities.

Conflicts of interest

He, X. is an Editorial Board Member of the journal *Energy Materials*, and he is not involved in any steps of editorial processing, notably including reviewer selection, manuscript handling, or decision-making. The other authors declare that there are no conflicts of interest.

Ethical approval and consent to participate

Not applicable.

Consent for publication

Not applicable.

REFERENCES

1. Zhang, Y.; Yang, Z.; Tian, C. Probing and quantifying cathode charge heterogeneity in Li ion batteries. *J. Mater. Chem. A.* **2019**, *7*, 23628-61. DOI
2. Yan, Z.; Wang, L.; Zhang, H.; He, X. Determination and engineering of Li-ion tortuosity in electrode toward high performance of Li-ion batteries. *Adv. Energy. Mater.* **2024**, *14*, 2303206. DOI
3. Srivastava, I.; Bolintineanu, D. S.; Lechman, J. B.; Roberts, S. A. Controlling binder adhesion to impact electrode mesostructures and transport. *ACS. Appl. Mater. Interfaces.* **2020**, *12*, 34919-30. DOI PubMed
4. Stallard, J. C.; Wheatcroft, L.; Booth, S. G.; et al. Mechanical properties of cathode materials for lithium-ion batteries. *Joule* **2022**, *6*, 984-1007. DOI
5. Kabra, V.; Carter, R.; Li, M.; et al. Lithium plating characteristics in high areal capacity Li-ion battery electrodes. *ACS. Appl. Mater. Interfaces.* **2024**, *16*, 34830-9. DOI
6. Li, Y.; Cao, Z.; Wang, Y.; et al. New insight into the role of fluoro-ethylene carbonate in suppressing Li-trapping for Si anodes in lithium-ion batteries. *ACS. Energy. Lett.* **2023**, *8*, 4193-203. DOI
7. Cha, H.; Kim, J.; Lee, H.; et al. Boosting reaction homogeneity in high-energy lithium-ion battery cathode materials. *Adv. Mater.* **2020**, *32*, 2003040. DOI

8. Gao, X.; Zhou, Y.; Han, D.; et al. Thermodynamic understanding of Li-dendrite formation. *Joule* **2020**, *4*, 1864-79. DOI
9. Duan, X.; Li, B.; Li, J.; Gao, X.; Wang, L.; Xu, J. Quantitative understanding of lithium deposition-stripping process on graphite anodes of lithium-ion batteries. *Adv. Energy. Mater.* **2023**, *13*, 2203767. DOI
10. Song, Y.; Wang, L.; Sheng, L.; et al. The significance of mitigating crosstalk in lithium-ion batteries: a review. *Energy. Environ. Sci.* **2023**, *16*, 1943-63. DOI
11. Mallick, S.; Gayen, D. Thermal behaviour and thermal runaway propagation in lithium-ion battery systems - a critical review. *J. Energy. Storage.* **2023**, *62*, 106894. DOI
12. Yan, Z.; Wang, L.; He, X. Rational electrode design for enhanced battery performance: addressing SOC heterogeneity and achieving energy density. *Adv. Funct. Mater.* **2025**, *35*, 2415637. DOI
13. Liu, H.; Kazemiabnavi, S.; Grenier, A.; et al. Quantifying reaction and rate heterogeneity in battery electrodes in 3D through operando X-ray diffraction computed tomography. *ACS. Appl. Mater. Interfaces.* **2019**, *11*, 18386-94. DOI
14. Strobridge, F. C.; Orvananos, B.; Croft, M.; et al. Mapping the inhomogeneous electrochemical reaction through porous $LiFePO_4$ - electrodes in a standard coin cell battery. *Chem. Mater.* **2015**, *27*, 2374-86. DOI
15. Sasaki, T.; Villevieille, C.; Takeuchi, Y.; Novák, P. Understanding Inhomogeneous reactions in Li-ion batteries: operando synchrotron X-Ray diffraction on two-layer electrodes. *Adv. Sci.* **2015**, *2*, 1500083. DOI PubMed PMC
16. Wolfman, M.; Khawaja, S.; Cabana, J. Mapping and metastability of heterogeneity in $LiMn_2O_4$ battery electrodes with high energy density. *J. Electrochem. Soc.* **2020**, *167*, 020526. DOI
17. Graae, K. V.; Li, X.; Etter, M.; Schökel, A.; Norby, P. Operando space-resolved inhomogeneity in lithium diffusion across NMC and graphite electrodes in cylinder-type Li-ion batteries. *J. Energy. Storage.* **2023**, *74*, 109523. DOI
18. Mikheenkova, A.; Schökel, A.; Smith, A. J.; et al. Visualizing ageing-induced heterogeneity within large prismatic lithium-ion batteries for electric cars using diffraction radiography. *J. Power. Sources.* **2024**, *599*, 234190. DOI
19. Judge, W. J.; May, B. M.; Kumar, K.; et al. Evaluation of chemical and structural homogeneity in single particles of $Li_{1-x}Ni_{0.33}Mn_{0.33}Co_{0.33}O_2$. *J. Phys. Chem. C.* **2022**, *126*, 16082-9. DOI
20. Sun, G.; Yu, F. D.; Lu, M.; et al. Surface chemical heterogeneous distribution in over-lithiated $Li_{1+x}CoO_2$ electrodes. *Nat. Commun.* **2022**, *13*, 6464. DOI PubMed PMC
21. Monasterial, A. P.; Weddle, P. J.; Atkinson, K.; et al. Dynamic in-plane heterogeneous and inverted response of graphite to fast charging and discharging conditions in lithium-ion pouch cells. *Small. Sci.* **2023**, *3*, 2200067. DOI
22. Kimura, Y.; Tomura, A.; Fakkao, M.; et al. 3D operando imaging and quantification of inhomogeneous electrochemical reactions in composite battery electrodes. *J. Phys. Chem. Lett.* **2020**, *11*, 3629-36. DOI
23. Nakamura, T.; Chiba, K.; Fakkao, M.; et al. Operando observation of formation and annihilation of inhomogeneous reaction distribution in a composite electrode for lithium-ion batteries. *Batteries. Supercaps.* **2019**, *2*, 688-94. DOI
24. Nakamura, T.; Watanabe, T.; Kimura, Y.; et al. Visualization of Inhomogeneous reaction distribution in the model $LiCoO_2$ composite electrode of lithium ion batteries. *J. Phys. Chem. C.* **2017**, *121*, 2118-24. DOI
25. Katayama, M.; Sumiwaka, K.; Miyahara, R.; et al. X-ray absorption fine structure imaging of inhomogeneous electrode reaction in $LiFePO_4$ lithium-ion battery cathode. *J. Power. Sources.* **2014**, *269*, 994-9. DOI
26. Tian, C.; Xu, Y.; Nordlund, D.; et al. Charge heterogeneity and surface chemistry in polycrystalline cathode materials. *Joule* **2018**, *2*, 464-77. DOI
27. Gent, W. E.; Li, Y.; Ahn, S.; et al. Persistent state-of-charge heterogeneity in relaxed, partially charged $Li_{1-x}Ni_{1/3}Co_{1/3}Mn_{1/3}O_2$ secondary particles. *Adv. Mater.* **2016**, *28*, 6631-8. DOI
28. Sun, T.; Sun, G.; Yu, F.; et al. Soft X-ray ptychography chemical imaging of degradation in a composite surface-reconstructed Li-rich cathode. *ACS. Nano.* **2021**, *15*, 1475-85. DOI
29. Maisuradze, M.; Li, M.; Mullaliu, A.; et al. Mapping heterogeneity of pristine and aged Li- and Na-mnhcf cathode by synchrotron-based energy-dependent full field transmission X-ray microscopy. *Small. Methods.* **2023**, *7*, 2300718. DOI
30. Fang, S.; Yan, M.; Hamers, R. J. Cell design and image analysis for in situ Raman mapping of inhomogeneous state-of-charge profiles in lithium-ion batteries. *J. Power. Sources.* **2017**, *352*, 18-25. DOI
31. Gilbert, J. A.; Maroni, V. A.; Cui, Y.; Gosztola, D. J.; Miller, D. J.; Abraham, D. P. Composition and impedance heterogeneity in oxide electrode cross-sections detected by raman spectroscopy. *Adv. Mater. Interfaces.* **2018**, *5*, 1701447. DOI
32. Kerlau, M.; Marcinek, M.; Srinivasan, V.; Kostecki, R. M. Reprint of "studies of local degradation phenomena in composite cathodes for lithium-ion batteries". *Electrochim. Acta.* **2007**, *53*, 1385-92. DOI
33. Davis, A. L.; Goel, V.; Liao, D. W.; et al. Rate limitations in composite solid-state battery electrodes: revealing heterogeneity with *operando* microscopy. *ACS. Energy. Lett.* **2021**, *6*, 2993-3003. DOI
34. Zhu, X.; Revilla, R. I.; Hubin, A. Direct correlation between local surface potential measured by kelvin probe force microscope and electrochemical potential of $LiNi_{0.80}Co_{0.15}Al_{0.05}O_2$ cathode at different state of charge. *J. Phys. Chem. C.* **2018**, *122*, 28556-63. DOI
35. Choi, S.; Toaran, W.; Kim, S. H.; Song, Y. J.; Kim, Y. Probing depth-dependent inhomogeneous lithium concentration in thick $LiNi_{0.88}Co_{0.09}Al_{0.03}O_2$ cathodes for lithium-ion batteries. *J. Alloys. Compd.* **2023**, *943*, 169029. DOI
36. Wood, V. X-ray tomography for battery research and development. *Nat. Rev. Mater.* **2018**, *3*, 293-5. DOI
37. Zhao, H.; Deng, H. D.; Cohen, A. E.; et al. Learning heterogeneous reaction kinetics from X-ray videos pixel by pixel. *Nature* **2023**, *621*, 289-94. DOI PubMed PMC
38. Wang, Y.; Feng, X.; Guo, D.; et al. Temperature excavation to boost machine learning battery thermochemical predictions. *Joule* **2024**,

8, 2639-51. DOI

39. Kosfeld, M.; Westphal, B.; Kwade, A. Moisture behavior of lithium-ion battery components along the production process. *J. Energy. Storage.* **2023**, *57*, 106174. DOI
40. Ng, S. H.; La, M. F.; Novák, P. A multiple working electrode for electrochemical cells: a tool for current density distribution studies. *Angew. Chem. Int. Ed.* **2009**, *48*, 528-32. DOI
41. Landesfeind, J.; Ebner, M.; Eldiven, A.; Wood, V.; Gasteiger, H. A. Tortuosity of battery electrodes: validation of impedance-derived values and critical comparison with 3D tomography. *J. Electrochem. Soc.* **2018**, *165*, A469. DOI
42. Ebner, M.; Chung, D.; García, R. E.; Wood, V. Tortuosity anisotropy in lithium-ion battery electrodes. *Adv. Energy. Mater.* **2014**, *4*, 1301278. DOI
43. Norris, C.; Parmananda, M.; Roberts, S. A.; Mukherjee, P. P. Probing the influence of multiscale heterogeneity on effective properties of graphite electrodes. *ACS. Appl. Mater. Interfaces.* **2022**, *14*, 943-53. DOI PubMed
44. Guo, Y.; Li, X.; Guo, H.; et al. Visualization of concentration polarization in thick electrodes. *Energy. Storage. Mater.* **2022**, *51*, 476-85. DOI
45. Klink, S.; Schuhmann, W.; La, M. F. Vertical distribution of overpotentials and irreversible charge losses in lithium ion battery electrodes. *ChemSusChem* **2014**, *7*, 2159-66. DOI PubMed
46. Yang, X.; Wang, C. Understanding the trilemma of fast charging, energy density and cycle life of lithium-ion batteries. *J. Power. Sources.* **2018**, *402*, 489-98. DOI
47. Attia, P. M.; Bills, A.; Brosa, P. F.; et al. Review-"knees" in lithium-ion battery aging trajectories. *J. Electrochem. Soc.* **2022**, *169*, 060517. DOI
48. Gao, T.; Han, Y.; Fraggedakis, D.; et al. Interplay of lithium intercalation and plating on a single graphite particle. *Joule* **2021**, *5*, 393-414. DOI
49. Li, B.; Chao, Y.; Li, M.; et al. A review of solid electrolyte interphase (SEI) and dendrite formation in lithium batteries. *Electrochem. Energy. Rev.* **2023**, *6*, 7. DOI
50. Paul, P. P.; Thampy, V.; Cao, C.; et al. Quantification of heterogeneous, irreversible lithium plating in extreme fast charging of lithium-ion batteries. *Energy. Environ. Sci.* **2021**, *14*, 4979-88. DOI